

Weak itinerant ferromagnetism and electronic and crystal structures of alkali-metal iron antimonides: $\text{NaFe}_4\text{Sb}_{12}$ and $\text{KFe}_4\text{Sb}_{12}$

A. Leithe-Jasper,* W. Schnelle, H. Rosner, M. Baenitz, A. Rabis, A. A. Gippius,† E. N. Morozova,‡ H. Borrmann, U. Burkhardt, R. Ramlau, U. Schwarz, J. A. Mydosh,‡ and Y. Grin
Max-Planck-Institut für Chemische Physik fester Stoffe, Nöthnitzer Str. 40, 01187 Dresden, Germany

V. Ksenofontov and S. Reiman

Institut für Anorganische Chemie und Analytische Chemie, Johannes-Gutenberg-Universität Mainz, Staudinger-Weg 9, 55099 Mainz, Germany

(Received 14 May 2004; revised manuscript received 13 August 2004; published 17 December 2004)

The synthesis, chemical, structural, and magnetic properties of alkali-metal compounds with filled-skutterudite structure, $\text{NaFe}_4\text{Sb}_{12}$ and $\text{KFe}_4\text{Sb}_{12}$, are described. X-ray and neutron diffraction and elemental analysis established the crystal structure without defects and disorder on the cation site. The temperature and pressure dependence of the cubic unit cell of $\text{NaFe}_4\text{Sb}_{12}$ and the displacement parameter of Na are investigated. The electronic structure is calculated by density functional methods (LMTO, FPLO). Quantum chemical calculations (electron localization function) reveal the covalent character of both Fe-Sb and Sb-Sb interactions. Electronic structure calculations within the local density approximation exhibit a band ferromagnetic ground state and predict a half-metallic behavior. In contrast to isostructural alkaline-earth compounds ($\text{CaFe}_4\text{Sb}_{12}$ and $\text{BaFe}_4\text{Sb}_{12}$), the alkali-metal skutterudites are itinerant electron ferromagnets with small magnetic moments ($\approx 0.25\mu_B/\text{Fe}$ atom) and $T_C \approx 85$ K. Yet the paramagnetic moments of all four compounds are between $1.5\mu_B$ and $1.7\mu_B$ per Fe atom, indicating similar Stoner factors. Temperature-dependent ^{57}Fe and ^{121}Sb Mössbauer spectroscopies confirm the ferromagnetic state in the sodium compound with very small hyperfine fields at the iron and antimony sites.

DOI: 10.1103/PhysRevB.70.214418

PACS number(s): 75.50.Bb, 75.40.Cx, 71.20.Lp, 76.80.+y

I. INTRODUCTION

The class of compounds known as “skutterudites” exhibits a wealth of topical behaviors, which are the source and motivation of increasing interest and efforts to study and understand the underlying physics. All these materials derive from the archetypal mineral skutterudite (CoAs_3).¹ Binary skutterudites having the general chemical formula TX_3 are formed by the members of the ninth group of the periodic system $T=(\text{Co}, \text{Rh}, \text{Ir})$ with pnictogens $X=(\text{P}, \text{As}, \text{Sb})$. No binary compounds with iron, ruthenium, and osmium could be synthesized under equilibrium conditions. In order to stabilize such compounds it is necessary to include electropositive elements as a third component leading to the total formula $R_yT_4X_{12}$ (filled skutterudites²). Here, R can be an alkaline-earth, rare-earth, and actinide metal or thallium. Different degrees of filling y can be realized up to $y=1$; however, the real limits for y depend strongly on the “filler” R and the “host” T_4X_{12} and are not yet well explored. These compounds $R_yT_4X_{12}$ are called “filled” since the stabilizing atoms reside in large voids already present in the transition-metal pnictogen framework (see Ref. 2 and Fig. 3).

A variety of properties has been observed for rare-earth-filled skutterudites ranging from metal-insulator transitions to magnetic and quadrupole orderings, conventional and unconventional superconductivity, heavy fermion and non-Fermi liquids, and fluctuating and mixed valency.^{3–6} Furthermore, interest in these compounds is fueled by their possible use in thermoelectric applications.^{7,8} For exhaustive reviews on the skutterudite physics and chemistry we refer to Refs. 3

and 8. All these studies suggest that the physics of filled skutterudites is governed by a subtle interplay of the filler ions and their surrounding transition-metal pnictogen host structure.

In order to gain a better understanding of these processes and to explore non-rare-earth skutterudites, we have successfully synthesized new alkali-metal compounds with sodium and potassium.⁹ The filler atoms are s -electron metals of small mass that are not magnetic and, therefore, are a good choice for the investigation of the d -electron influence on the properties of filled skutterudites.

In this article, we present our investigations of the recently synthesized skutterudites $\text{NaFe}_4\text{Sb}_{12}$ and $\text{KFe}_4\text{Sb}_{12}$. These materials exhibit bulk ferromagnetic transitions at $T_C \approx 85$ K with weak itinerant iron magnetic moments and strong spin fluctuations.⁹ We propose that these compounds belong to the class of half-metallic ferromagnets,¹⁰ which are promising materials for spin-electronic devices (spintronics). We compare them with the alkaline-earth (Ca, Ba) compounds previously studied by Danebrock, Evers, and Jeitschko¹¹ which remain paramagnetic down to helium temperatures.

Section II will describe our experimental techniques, regarding synthesis, structural, and physical properties and the calculational methods of electron localization function (ELF) and band structure. In Sec. III we show results for the crystal structure, chemical bonding, and electronic band structure along with the magnetic properties of the two ferromagnetic compounds (Na and $\text{KFe}_4\text{Sb}_{12}$) and the isostructural Ca and Ba skutterudites. ^{57}Fe and ^{121}Sb Mössbauer spectroscopy for

$\text{NaFe}_4\text{Sb}_{12}$ is employed to determine the hyperfine splitting in the ferromagnetic ground state of the sodium compound. Finally, Sec. IV summarizes the results.

II. EXPERIMENT

A. Synthesis

Due to the high vapor pressure of the alkali metals, polycrystalline samples of $\text{NaFe}_4\text{Sb}_{12}$ and $\text{KFe}_4\text{Sb}_{12}$ were prepared in a two-step synthesis. First, the binary compounds NaSb and KSb were synthesized from the elements (Na, K, 99.99% from ABCR; Sb, shot, 99.99% ChemPur) in a sealed tantalum ampoule. Then, a stoichiometric mixture of powdered alkali-metal monoantimonides together with FeSb_2 (Fe, powder, 99.9% ChemPur) and elemental Sb was compacted to a pellet which was annealed in a sealed Ta ampoule at 400 °C for 1 week, followed by regrinding and additional heat treatment cycles. Since binary alkali-metal antimony compounds are very sensitive to air, all these steps were carried out in an argon-filled glove box with oxygen and moisture content less 1 ppm.

The ternary compounds were obtained as dark gray powders. In contrast to the educts, they are not at all sensitive to air or moisture. The compounds $\text{CaFe}_4\text{Sb}_{12}$ and $\text{BaFe}_4\text{Sb}_{12}$ were synthesized in a similar manner. Compacted blends of FeSb_2 , Sb, CaSb_2 , and BaSb_2 , respectively, were annealed at 500 °C in sealed Ta tubes.

Single-crystal grains of $\text{NaFe}_4\text{Sb}_{12}$ could be isolated from a sample which was heated to 700 °C and furnace cooled in order to obtain larger grains. Physical properties measurements were performed on specimens cut from compacted samples which were prepared by spark plasma sintering¹² (SPS) the powders at 200 °C and at a pressure of 600 MPa for 3 h under an atmosphere of argon. In this way, 92% of the theoretical density of the bulk material could be achieved.

Metallographic microstructure analyses on polished surfaces were performed with optical microscopy and electron-probe microanalysis (EPMA). The latter investigations were done with a wavelength-dispersive (WDX) Cameca SX100 system. Elemental standards for iron and antimony and NaCl as a sodium standard were used. Energy-dispersive analysis (EDX) of the samples was carried out in a Philips XL30 scanning electron microscope. These investigations revealed elementary antimony as a common impurity phase (about 2 vol. %) present after SPS treatment.

Magnetization measurements (see below) showed that as-synthesized powders and SPS-treated samples contained a ferromagnetic impurity with a Curie temperature well above 400 K. This impurity is most probably metallic iron ($T_C = 1043$ K). The content is some 100 $\mu\text{g/g}$, well below the detection limits of conventional analytical methods. Batches of skutterudite material were therefore finely powdered, etched in hydrochloric acid (HCl; 20%), and rinsed in distilled water repeatedly. This treatment strongly reduced the amount of ferromagnetic impurities.

B. Structure investigations

Powder x-ray diffraction (XRD) measurements were made using $\text{Cu } K\alpha_1$ radiation ($\lambda = 1.54060$ Å) applying the

Guinier Huber technique using LaB_6 as an internal standard ($a = 4.15692$ Å). Low-temperature powder XRD was performed on a Huber Guinier camera with a sample holder incorporated in a closed-cycle helium cryostat. For correct lattice parameter determination, the measurement was performed with silicon powder ($a = 5.4311946$ Å) used as an internal standard.¹³ Powder neutron diffraction data were collected at the Hahn-Meitner-Institut, Berlin, with instrument E9. Single-crystal data were collected on a Stoe IPDS system (Ag $K\alpha$ radiation; $\lambda = 0.56086$ Å) and on a Rigaku R-axis RAPID diffractometer (Mo $K\alpha$ radiation 0.71073 Å). Crystallographic calculations were made with the WINCSD (Ref. 14) and the SHELXL-97 (Ref. 15) program packages.

C. Physical properties

Magnetic properties were measured on a superconducting quantum interference device (SQUID) magnetometer (MPMS XL-7, Quantum Design). Zero-field cooling (ZFC, measured in warming) and field-cooling (FC) runs and isothermal magnetization loops were performed up to $H_{\text{ext}} = 70$ kOe. Additional isothermal magnetization curves up to $H_{\text{ext}} = 140$ kOe were measured by an extraction technique (PPMS, Quantum Design). No demagnetization or diamagnetic core corrections were applied.

Mössbauer measurements of powder samples of $\text{NaFe}_4\text{Sb}_{12}$ were performed in a transmission geometry using a constant-acceleration spectrometer and a helium bath cryostat. ^{57}Fe Mössbauer spectra were recorded at room temperature and 4.2 K using the 50 mCi source $^{57}\text{Co}(\text{Rh})$. The RECOIL 1.03 Mössbauer analysis software was used to fit the experimental spectra.¹⁶ Isomer shift values are quoted relative to $\alpha\text{-Fe}$ at 293 K. For Sb Mössbauer spectroscopy, a $^{121\text{m}}\text{Sn}(\text{CaSnO}_3)$ source with an activity of 3.0 mCi was placed together with the absorber in the helium bath cryostat. The spectra were analyzed with the program EFFI (Ref. 17) using the transmission integral. During the fit the source recoil-free fraction value was kept 0.6.

D. Calculation procedures

Linear muffin-tin orbital (LMTO) method. The tight-binding (TB) LMTO atomic sphere approximation (ASA) program package¹⁸ with exchange correlation potential [local density approximation (LDA)] according to Barth and Hedin¹⁹ was used for quantum chemical calculations on $\text{NaFe}_4\text{Sb}_{12}$. The radial scalar-relativistic Dirac equation was solved to obtain the partial waves. Although the calculation within the ASA includes corrections for the neglect of interstitial regions and partial waves of higher order,²⁰ an addition of empty spheres in the case of $\text{NaFe}_4\text{Sb}_{12}$ was not necessary. The following radii of atomic spheres were used: $r(\text{Na}) = 2.642$ Å, $r(\text{Fe}) = 1.528$ Å, and $r(\text{Sb}) = 1.714$ Å. A basis set containing $\text{Na}(3s)$, $\text{Fe}(4s, 4p, 3d)$, and $\text{Sb}(5s, 5p)$ orbitals was employed for the self-consistent calculations with the $\text{Na}(3p, 3d)$ and $\text{Sb}(5d, 5f)$ functions being downfolded. The calculation was performed spin-polarized.

Electron localization function (ELF). The ELF was evaluated according to Savin *et al.*^{21,22} with an ELF module al-

TABLE I. Crystallographic data of cubic $\text{NaFe}_4\text{Sb}_{12}$ at different temperatures. Structure type: $\text{LaFe}_4\text{P}_{12}$. Space group: $Im\bar{3}$, $Z=2$. Na is in $2a$ (0,0,0); Fe in $8c$ ($\frac{1}{4}, \frac{1}{4}, \frac{1}{4}$). Sb in $24g$ (0, y , z).

T [K]	a [Å]	Coordinates		Displacement parameters			Interatomic distances		
		y	z	$U_{\text{Na}}^{\text{iso}}$	$U_{\text{Fe}}^{\text{iso}}$ [10^{-3}Å^2]	$U_{\text{Sb}}^{\text{iso}}$	d_1, d_2 (Sb-Sb) [Å]	d (Fe-Sb) [Å]	d (Na-Sb) [Å]
295 ^a	9.1767(5)	0.1588(1)	0.3369(1)	22.0(3)	3.5(3)	5.3(4)	2.99(1), 2.91(1)	2.57(1)	3.417(1)
300 ^b	9.1759(3)	0.1593(4)	0.3363(4)	41(5)	4.4(6)	6.5(5)	3.00(1), 2.93(1)	2.57(2)	3.415(4)
50 ^b	9.1541(5)	0.1584(4)	0.3362(4)	13(3)	5.2(4)	4.3(6)	3.00(1), 2.91(1)	2.56(1)	3.406(4)
2 ^b	9.1524(2)	0.1588(4)	0.3369(4)	8(3)	3.7(5)	3.2(5)	2.99(1), 2.91(1)	2.56(2)	3.409(4)

^aFrom room-temperature single-crystal XRD data: $R=0.014$, $wR_2=0.025$.

^bFrom powder neutron diffraction data: $T=300$ K: $R_1=0.041$, $R_p=0.12$. $T=50$ K: $R_1=0.042$, $R_p=0.12$. $T=2$ K: $R_1=0.039$, $R_p=0.11$.

ready implemented within the TB-LMTO-ASA program package.¹⁸ To gain a deeper insight in the chemical bonding, the topology of the ELF was analyzed with the program BASIN.²³ The electron density was integrated in the basins which are bounded by zero flux surfaces in the ELF gradient field. This method, analogous to the procedure proposed by Bader for the electron density,²⁴ gave electron counts for each basin, which reveal basic information for the description of the bonding situation.

Full-potential local-orbital (FPLO) scheme. To obtain more accurate total energies and detailed electronic structure information, in addition, a full-potential nonorthogonal local-orbital calculation scheme²⁵ within the L(S)DA was used. In the scalar-relativistic calculations the exchange and correlation potentials of Perdew and Wang²⁶ were used. As the basis set, $\text{Na}(2s, 2p, 3s, 3p, 3d)$, $\text{Fe}(3s, 3p, 4s, 4p, 3d)$, and $\text{Sb}(4s, 4p, 4d, 5s, 5p, 5d)$ states were employed. The lower-lying states were treated fully relativistically as core states. The Na $3d$ states as well as the Sb $5d$ states were taken into account as polarization states to increase the completeness of the basis set. The treatment of the $\text{Na}(2s, 2p)$, $\text{Fe}(3s, 3p)$, and $\text{Sb}(4s, 4p, 4d)$ semicorelike states as valence states was necessary to account for non-negligible core-core overlaps. The spatial extension of the basis orbitals, controlled by a confining potential $(r/r_0)^4$, was optimized to minimize the total energy.²⁷ A k mesh of 396 points in the irreducible part of the Brillouin zone (8000 in the full zone) was used to ensure accurate density of states and band structure information, especially in the region close to the Fermi level.

III. RESULTS AND DISCUSSION

A. Crystal structure

Powder XRD data give cubic lattice parameters $a = 9.1767(5)$ Å for $\text{NaFe}_4\text{Sb}_{12}$ and $a = 9.1994(5)$ Å for $\text{KFe}_4\text{Sb}_{12}$, respectively. These values are larger than those in $\text{CaFe}_4\text{Sb}_{12}$ [$a = 9.1634(4)$ Å; cf. $a = 9.162(1)$ Å (Ref. 28)] but smaller than for $\text{BaFe}_4\text{Sb}_{12}$ [$a = 9.2058(2)$ Å; cf. $a = 9.202(2)$ Å (Ref. 28); $a = 9.200(3)$ Å (Ref. 29)]. Single-crystal XRD analysis (see Table I) of $\text{NaFe}_4\text{Sb}_{12}$ corroborates the full occupancy (100%) of the $2a$ site by sodium. The refinement of the occupancy for the sodium position does not improve the residual values in comparison with the full oc-

cupancy. Iron and antimony positions also do not show any deviation from full occupancy. This result is also confirmed by WDX analysis of a polished surface of the sample from which the single crystal for structure analysis was selected. The composition $\text{Na}_{0.95(1)}\text{Fe}_{4.08(1)}\text{Sb}_{11.29(1)}$ is obtained. Additionally, the WDX-EPMA of SPS-treated bulk samples gives a composition of $\text{Na}_{0.97(3)}\text{Fe}_{4.06(2)}\text{Sb}_{11.95(3)}$ and $\text{K}_{0.98(1)}\text{Fe}_{4.05(2)}\text{Sb}_{11.97(3)}$, respectively.

At room temperature sodium shows a large displacement parameter (see Table I). Since the chemical analysis of our material gives no evidence of partial occupation, we can rule out defects on this position on the level of 3%.

In order to obtain more information about the displacement factors, the crystal structure of $\text{NaFe}_4\text{Sb}_{12}$ as a function of temperature was investigated from powder neutron diffraction data (see Table I). The atomic displacement parameter $U_{\text{iso}} = B_{\text{iso}}/8\pi^2$ of Na is strongly temperature dependent, while the values for Sb and Fe show only a weak dependence or almost no dependence on temperature, respectively. At 2 K the U_{iso} values for all three positions are of similar magnitude close to zero (Fig. 1). The difference between the displacement parameters for Na and Fe (Sb) extrapolated to 0 K is less than 0.005Å^2 , which range roughly 3 mean e.s.d. This reveals only the conventional dynamic thermal motion (Einstein oscillator) of sodium atoms inside the slightly oversized antimony cage.

It has been speculated that the skutterudites are therefore prone to various kinds of displacive-type phase transitions^{28,30} where at lower temperatures the configuration becomes increasingly unstable due to freezing of the thermal motion of the filler atoms³¹ which might then lock-in to off-center positions in the cages^{28,30} and, thus, possibly induce structural distortions which could lower the crystal symmetry. Indications of static off-center movement have been indeed found in metastable skutterudites filled with heavy rare earths.^{32,33} However, no indications of a lock-in-type phase transition were found for $\text{NaFe}_4\text{Sb}_{12}$. At room temperature, off-center displacements of the sodium atom can be ruled out due to the spherical distribution of the difference electron density³⁴ in the vicinity of the Na position (Fig. 2).

Thermal expansion of $\text{NaFe}_4\text{Sb}_{12}$ was studied by powder XRD (determination of the cubic lattice parameter) in the temperature range from 15 K to 300 K and is rather small. For the temperature range 100–300 K (with an approxi-

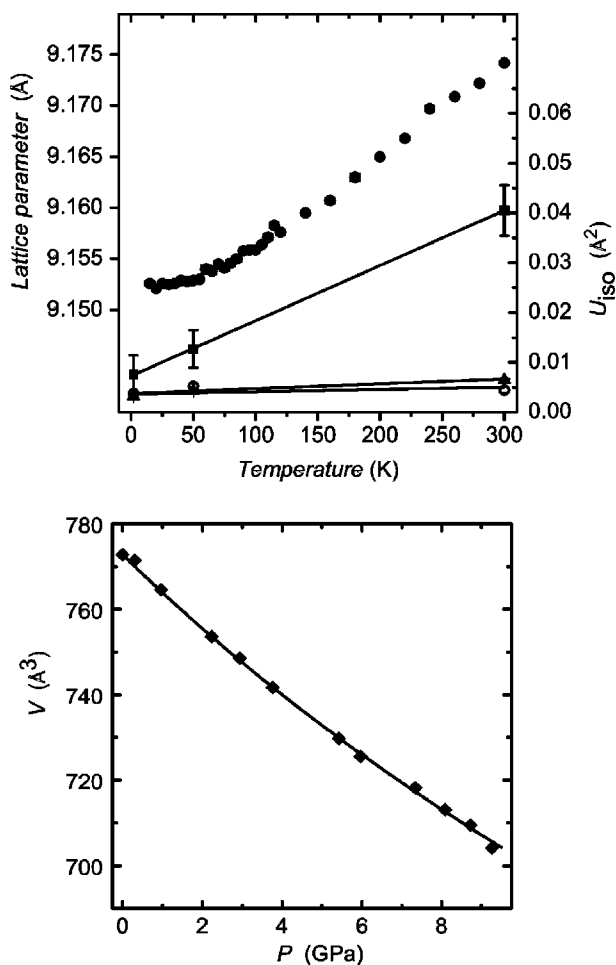


FIG. 1. Upper panel: temperature dependence of the cubic lattice parameter (●) for $\text{NaFe}_4\text{Sb}_{12}$ from the powder x-ray diffraction data. Isotropic displacement parameters U_{iso} for Na (squares), Fe (circles), and Sb (triangles) are displayed. Lower panel: pressure dependence of the unit cell volume. The line represents a fit of a Murnaghan equation of state.

mately linear slope of a) the coefficient of linear expansion $\alpha = 11 \times 10^{-6} \text{ K}^{-1}$ which is only slightly larger than $9 \times 10^{-6} \text{ K}^{-1}$ derived from neutron diffraction data for $\text{LaFe}_4\text{Sb}_{12}$.³¹ According to these data, the iron-antimony framework is rather rigid. Similar conclusions were drawn from lattice dynamics calculations.^{35,36} Also the high Debye temperature for the Os-Sb framework in $\text{PrOs}_4\text{Sb}_{12}$ [$\approx 375 \text{ K}$ (Ref. 33)] and for CoSb_3 [307 K (Ref. 37)] generally point to a rigid skutterudite lattice. No indications of possible structural transitions are found from the temperature dependence of the lattice parameters for $\text{NaFe}_4\text{Sb}_{12}$ (see Fig. 1 and the distances listed in Table I).

The pressure dependence of the unit cell volume of $\text{NaFe}_4\text{Sb}_{12}$ (Fig. 1) in the range up to 9.5 GPa is characteristic for intermetallic compounds. The least-squares fit of a Murnaghan-type equation of state³⁸ to the experimental data leads to the zero-pressure unit cell volume $V_0 = 772.78 \text{ \AA}^3$ and a bulk modulus (at $p=0$) $B_0 = 85(1) \text{ GPa}$ using $B'_0 = 4$ (fixed first derivative). A similar value of $B_0 = 88(4) \text{ GPa}$ was recently found for the intermetallic compound YbAgGa_2 with a covalently bonded polyanion $[\text{AgGa}_2]$.³⁹ A higher sta-

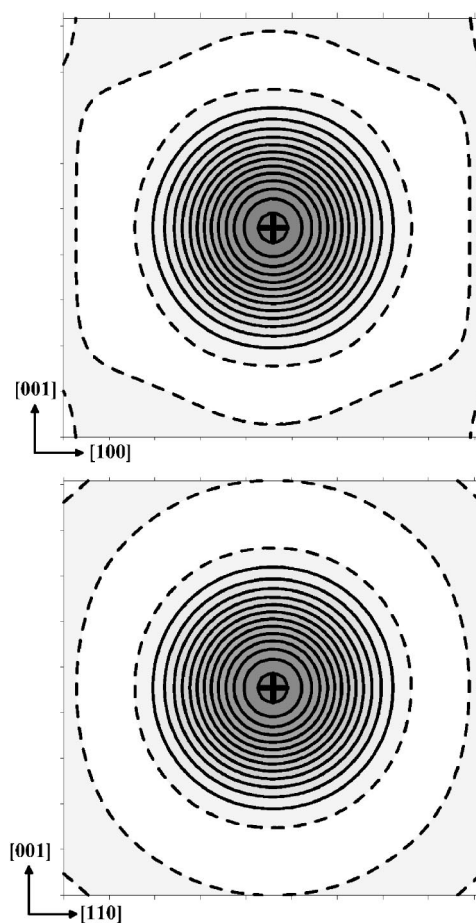


FIG. 2. Experimental difference electron density distribution around the Na position in $\text{NaFe}_4\text{Sb}_{12}$. “+” indicates the position of the sodium atom. Dashed lines show the zero level; the isolines are drawn with the step $5e^-/\text{\AA}^3$; the step width on each axis is 0.2 \AA .

bility of a skutterudite structure to compression [$B_0 = 136(5) \text{ GPa}$, $B'_0 = 4.8(5)$] was found for the binary compound IrSb_3 .⁴⁰

B. Chemical bonding and electronic structure

The electron localization function (ELF, η , normalized to values between 0 and 1) is an appropriate tool for the investigation of chemical bonding in real space^{21,22} and helps in understanding the nature of the atomic interactions. For more details we refer to Refs. 41 and 42.

The positions of the ELF maxima (attractors) visualize the direct interatomic bonds in the structure (real space). The topological analysis of the ELF of $\text{NaFe}_4\text{Sb}_{12}$ displays only three types of attractors in the valence region (see Fig. 3). Two of them are located on the shortest Sb-Sb contacts d_1 and d_2 in the Fe-Sb framework (cf. Table I and Fig. 3), confirming the covalent character of the interaction between the antimony atoms belonging to the neighboring $[\text{FeSb}_6]$ octahedrons. The third one is located slightly shifted off the Fe-Sb bond lines, showing a pronounced covalency of these bonds [Fig. 3(b)]. No unique attractors were found in the valence region in between the sodium and framework atoms (antimony or iron).

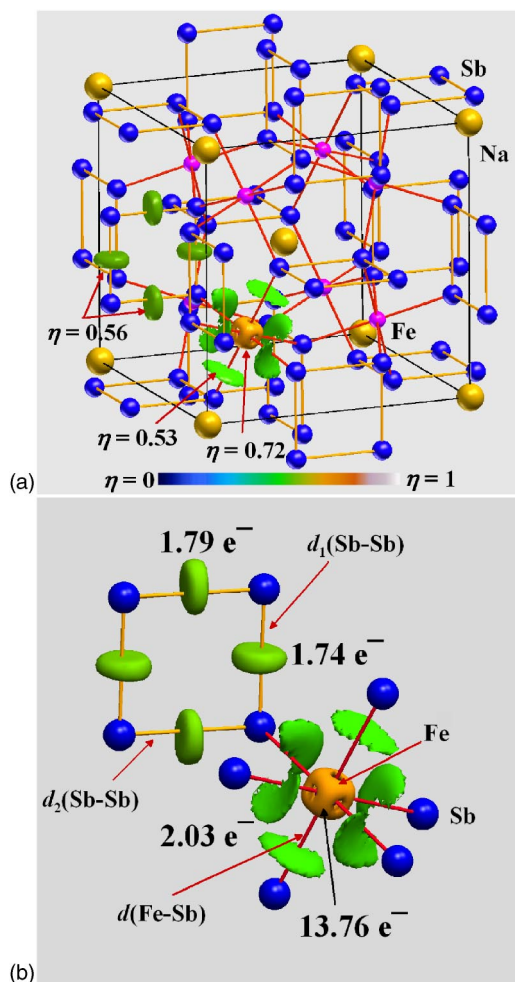


FIG. 3. (Color online) Electron localization function η for $\text{NaFe}_4\text{Sb}_{12}$. (a) Crystal structure of $\text{NaFe}_4\text{Sb}_{12}$ with shortest interatomic distances Fe-Sb and Sb-Sb. Isosurfaces of ELF illustrate the covalent interaction between Fe and Sb ($\eta=0.53$) and between antimony atoms ($\eta=0.56$). The isosurface with ($\eta=0.72$) shows the structuring of the third shell for the iron atoms; see text. (b) Electron counts for relevant bonds in the $\text{NaFe}_4\text{Sb}_{12}$ structure.

Each attractor has a so-called basin defined by zero-flux surfaces in the gradient field of ELF.⁴¹ The lowest ELF values on the border between two basins are called interconnect points. The lower the ELF value at the interconnecting point, the better the basins are separated; consequently, there exists a larger charge separation. The basin of the sodium inner shell interconnects with the framework basin only at a very low value of $\eta < 0.1$. Both facts—the absence of bonding attractors in the vicinity of sodium atoms and the clear charge separation—strongly suggest a charge transfer from sodium to the Fe-Sb framework. Another relevant topological feature of ELF in $\text{NaFe}_4\text{Sb}_{12}$ is the structuring of the inner shell of the iron atoms [see isosurface with $\eta=0.72$ in Fig. 3(b)]. According to Ref. 41 this suggests a participation of the inner-shell electrons of iron in the interactions in the valence region between the atoms.

Integration of the total electron density in the ELF basins for the Sb-Sb attractors gives electron counts of 1.74 and 1.79 for $d_1(\text{Sb-Sb})$ and $d_2(\text{Sb-Sb})$, respectively. For the Fe-

Sb contacts the count of 2.03 electrons was observed [Fig. 3(b)]. For the inner shell of the iron atoms, 13.76 electrons were found (instead of the 14 expected), which is in good agreement with the calculation for free atoms⁴³ and confirms the participation of the inner-shell electrons in the interactions in the valence region. For the core region of the sodium atoms 9.98 electrons were found from the integration procedure in good agreement with ten expected from the Aufbau principle for Na^+ . This would give a charge transfer of 1.02 electrons from each sodium to the polyanion. On the other hand, the polyanion $\text{Fe}_4\text{Sb}_{12}$ is formed by 6 Sb-Sb (d_1), 6 Sb-Sb (d_2), and 24 Fe-Sb bonds. This gives a total count of 69.90 electrons for the polyanion and suggests a charge transfer of 0.94 electrons from each sodium to the polyanion (subtracting $12 \times 5e^-$ of Sb and $4 \times 2.24e^-$ of Fe from $69.90e^-$). Both evaluation procedures give similar results; thus, the mean value of charge transfer is 0.98 electrons. Accordingly, the total electron balance can be written as $\text{Na}^{0.98+}[\text{Fe}_4\text{Sb}_{12}]^{0.98-}$.

Considering the strong overlap of the 3s band of Na with Sb 5p band in the density of states (DOS) (see below) and taking into account the rectangular arrangement of the Sb-Sb bonds in the structure (Fig. 3), we propose the transfer of the sodium charge to the Sb-Sb bonds. Further details will be discussed in a forthcoming publication about the chemical bonding and electronic structure in the skutterudites $M\text{Fe}_4\text{Sb}_{12}$ (M =alkali, alkaline-earth, or rare-earth metal).⁴⁴ Following the ELF representation, the whole structure of $\text{NaFe}_4\text{Sb}_{12}$ has to be considered as a three-dimensional covalently bonded polyanionic framework of iron and antimony atoms with sodium cations embedded into the cavities. This scenario is in good agreement with the rigidity of the structure found from the experimental thermal expansion and compressibility.

The significantly larger bulk modulus of IrSb_3 can be rationalized considering the larger number of electrons available for bonding in $[\text{Ir}_4\text{Sb}_{12}]^0$ in comparison with $[\text{Fe}_4\text{Sb}_{12}]^{0.98-}$.

The influence of this bonding mechanism on the magnetism and transport properties^{9,45} can be understood from the results of the band structure calculations. The density of states and band structure data for $\text{NaFe}_4\text{Sb}_{12}$ calculated by the LMTO and FPLO procedures are in good agreement.

Figure 4 shows the total as well as the partial Fe and Sb DOS from the spin-polarized calculation (FPLO) for $\text{NaFe}_4\text{Sb}_{12}$. Due to the high DOS value of 42 states $\text{eV}^{-1} \text{f.u.}^{-1}$ for the paramagnetic solution (see Fig. 5 in Ref. 9), spin splitting of the mainly Fe 3d-related states leads to a considerable reduction of the total energy (0.236 eV/f.u.), resulting in a ferromagnetic ground state with a magnetic moment of $2.97\mu_B$ per cell. The most striking feature on the DOS plot is the almost negligible contribution of the majority channel (DOS_\downarrow) at the Fermi level. It amounts to $0.1 \text{ eV}^{-1} \text{f.u.}^{-1}$ only, compared to $21.1 \text{ eV}^{-1} \text{f.u.}^{-1}$ for the minority states (DOS_\uparrow). This results in a spin polarization of $(\text{DOS}_\uparrow - \text{DOS}_\downarrow) / (\text{DOS}_\uparrow + \text{DOS}_\downarrow) = 0.99$, and thus, an almost perfect half-metallic behavior of the compound.

The results for the isovalent $\text{KFe}_4\text{Sb}_{12}$ compound are nearly identical. From the very similar features in the energy

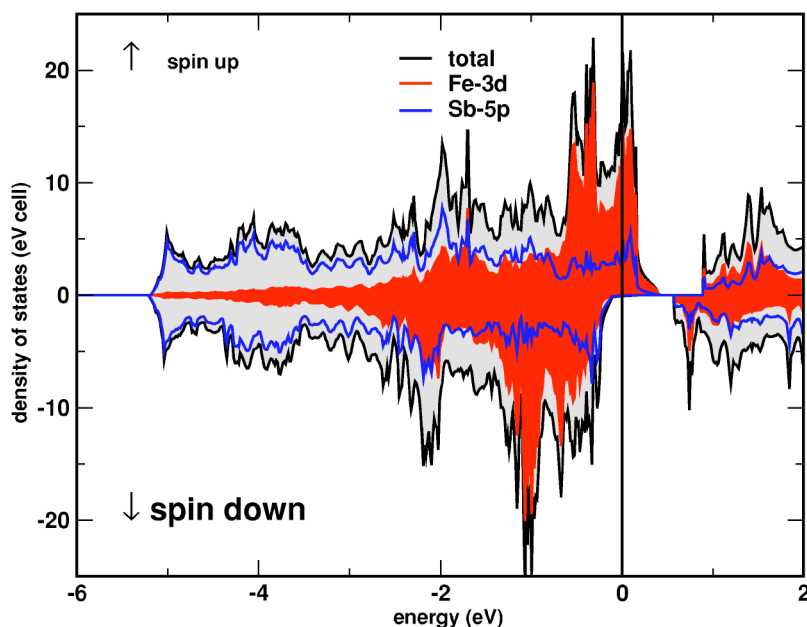


FIG. 4. (Color online) Total, Fe 3d, and Sb 5p derived density of states, respectively, for $\text{NaFe}_4\text{Sb}_{12}$ for the ferromagnetic state. The Fermi level is at zero energy.

region between -2 eV and 2 eV in the partial Fe 3d and Sb 5p DOS we can conclude a strong hybridization of these states (i.e., bonding) in agreement with the ELF results. This is also confirmed by “fat band analysis” of the Fe 3d and Sb 5p states (not shown). The Na (K) contribution to the occupied states is small. The Na 3s states overlap with Sb 5p states in the entire valence region (between -5 eV and E_F).

The corresponding spin-polarized band structure for the valence band region of $\text{NaFe}_4\text{Sb}_{12}$ is presented in Fig. 5. It shows that only one majority (\downarrow) band crosses the Fermi level, whereas five minority bands (\uparrow) contribute to the Fermi surface. The majority band (\downarrow) at the Fermi level is dominated by Sb 5p states, whereas the minority (\uparrow) bands are mainly due to Fe 3d. The high DOS for the minority channel results from the rather flat dispersion of the minority bands in parts of the Brillouin zone (see Fig. 5 around the H

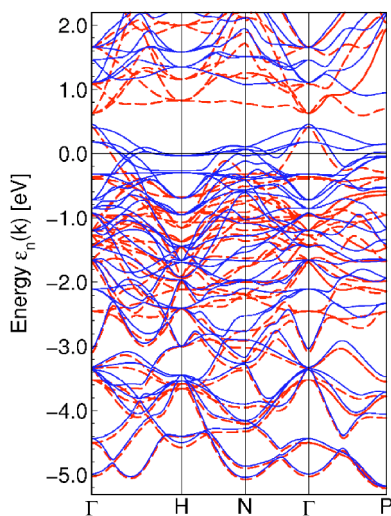


FIG. 5. (Color online) Band structure of $\text{NaFe}_4\text{Sb}_{12}$ for the ferromagnetic state; the Fermi level is at zero energy; the minority (\uparrow , solid lines) and majority bands (\downarrow , dashed lines).

point). For a comparative study of the influence of different filler cations on the electronic structure of skutterudites and the importance of spin fluctuations we refer to Ref. 44.

C. Magnetic properties

The magnetization $M(T)$ of SPS-compacted samples of $\text{NaFe}_4\text{Sb}_{12}$ and $\text{KFe}_4\text{Sb}_{12}$ in different external magnetic fields H_{ext} is displayed in Fig. 6. The new alkali-metal compounds order ferromagnetically at $T_C \approx 85$ K. The magnetization per Fe atom for both the Na and the K compound reaches about $0.52\mu_B$ at 1.8 K in the highest external field of the SQUID magnetometer (70 kOe). The gross features for the ZFC and FC curves in lower external fields are the same for both compounds: the ZFC and FC curves are indistinguishable for fields of 10 kOe and higher; thus, domain effects do not play an important role and the isotherms are reversible. However, the magnetic moment at 10 kOe is about 25%–30% less than in 70 kOe. For $H_{\text{ext}} = 1$ kOe and lower fields a clear ZFC-FC splitting is observed, typical for ferromagnetic domain effects. An interesting feature of the FC curve for $H_{\text{ext}} = 10$ kOe of $\text{KFe}_4\text{Sb}_{12}$ is that $M(T)$ decreases with decreasing temperature below 20 K. This effects was reproduced on a different SPS-treated bulk sample and on purified $\text{KFe}_4\text{Sb}_{12}$ powder. This unusual behavior exists only for $H_{\text{ext}} \approx 10$ kOe where $M(H)$ (see below) becomes reversible and is probably connected to domain effects.

Isothermal magnetization loops provide further information on the ferromagnetic state. For the current sample of $\text{NaFe}_4\text{Sb}_{12}$ (SPS, Fig. 7) the remanent moment M_r per Fe atom at 1.8 K is $0.25\mu_B$ which is slightly smaller than for the previously published sample⁹ ($0.28\mu_B$). $M(H)$ at 1.8 K increases smoothly with field and reaches $0.60\mu_B$ in $H_{\text{ext}} = 140$ kOe (sample from Ref. 9). The low remanent moment and the continuous increase with H_{ext} are due to strong spin fluctuations (see below). Almost identical $M(H)$ curves are found for as-prepared powder, purified powder, and SPS-

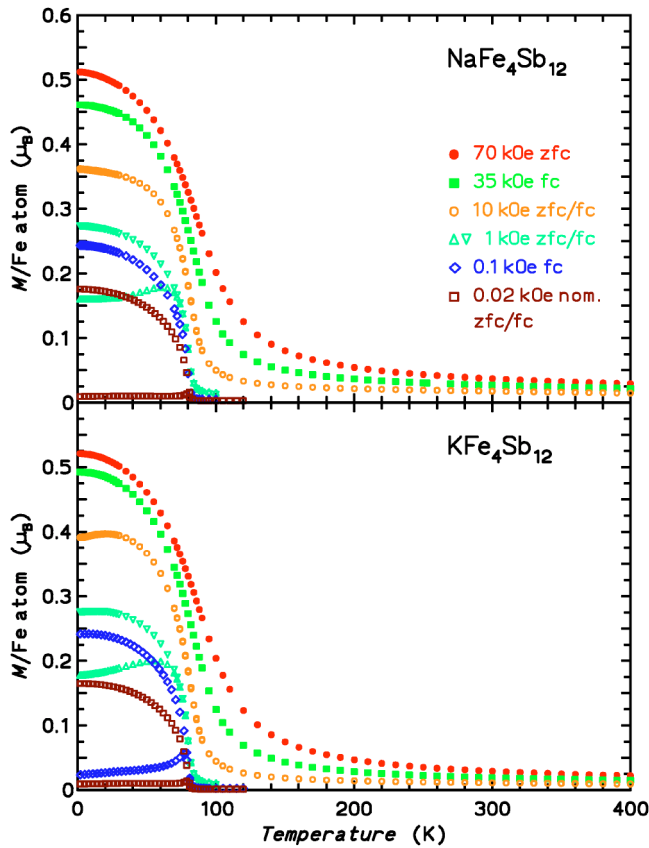


FIG. 6. (Color online) Magnetization per Fe atom versus temperature for different external magnetic fields H_{ext} for SPS-treated $\text{NaFe}_4\text{Sb}_{12}$ and $\text{KFe}_4\text{Sb}_{12}$. Generally, the lower-lying curves for a field are the ZFC runs. For $H_{\text{ext}}=1$ kOe, ZFC runs (Δ), FC runs (∇).

treated $\text{NaFe}_4\text{Sb}_{12}$ and $\text{KFe}_4\text{Sb}_{12}$ samples. The observed magnetic moment for $H_{\text{ext}}=140$ kOe ($0.60\mu_B$, and $0.65\mu_B$ when extrapolating M to $1/H \rightarrow 0$) is only little less than the moment obtained from fixed spin moment calculations

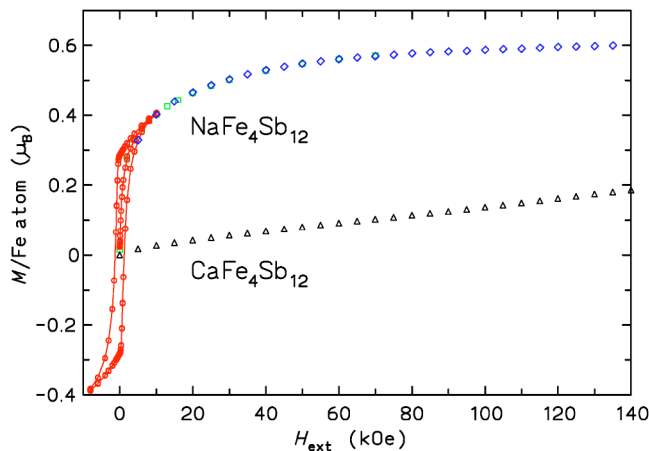


FIG. 7. (Color online) Isothermal magnetization ($T=1.8$ K) per Fe atom versus external magnetic field for SPS-treated $\text{NaFe}_4\text{Sb}_{12}$ (sample from Ref. 9) and non-SPS $\text{CaFe}_4\text{Sb}_{12}$ powder. Data below 70 kOe (SQUID magnetometer) and up to 140 kOe (extraction method) were combined.

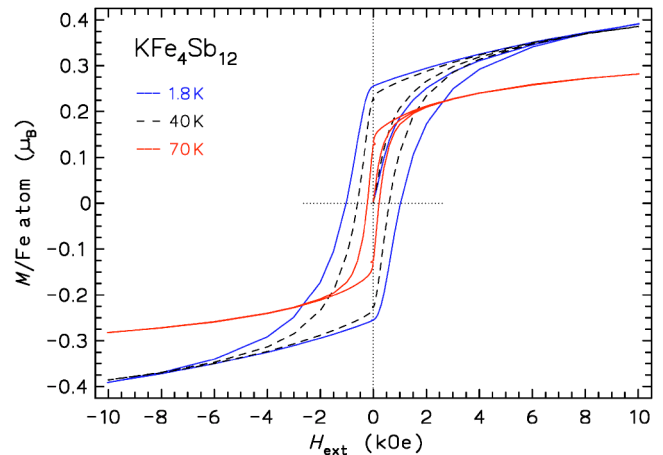


FIG. 8. (Color online) Magnetization per Fe atom versus external magnetic field for SPS-treated $\text{KFe}_4\text{Sb}_{12}$. Isotherms were registered for nine different temperatures out of which three are shown.

($0.74\mu_B$ per Fe atom⁹). The hysteresis curves close for external fields around 10 kOe (Fig. 8). For powder samples the magnetization loop is more rounded off (not shown), the coercive field is only ≈ 0.6 kOe (while $H_c \approx 1.2$ kOe for SPS samples), and the remanent moment is a little smaller due to the different ferromagnetic domain structure. With increasing temperature the magnetization loops become regularly smaller and narrower as demonstrated for SPS treated $\text{KFe}_4\text{Sb}_{12}$ in Fig. 8.

Data of the paramagnetic susceptibility of Fe-containing skutterudite materials^{11,46} where the filler cation does not have a magnetic moment are scarce. The data analysis is often hampered by the contribution of a ferromagnetic impurity. The inverse magnetic susceptibility H/M (Fig. 9) in the paramagnetic range can thus be significantly field dependent. Assuming a saturation of the magnetization of the ferromagnetic impurity in fields well above 10 kOe the susceptibility M/H of the skutterudite can be extrapolated from data taken

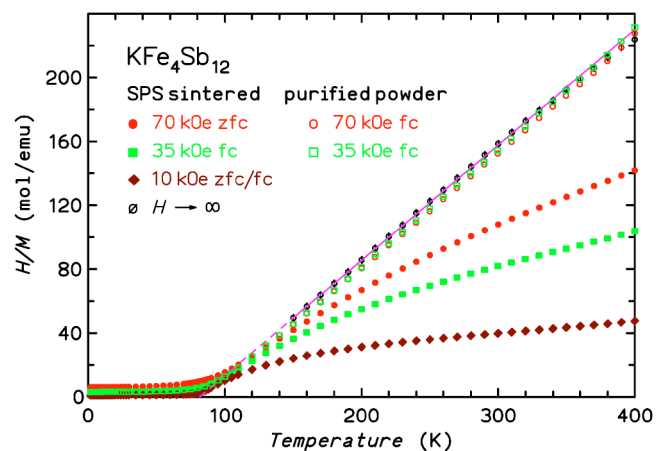


FIG. 9. (Color online) Inverse magnetic susceptibilities $H/M(T)$ for different external magnetic fields and extrapolated values ($H \rightarrow \infty$) for an SPS-treated sample and a purified powder sample of $\text{KFe}_4\text{Sb}_{12}$. The line represents the Curie-Weiss fit for the SPS bulk sample listed in Table II.

TABLE II. Results of Curie-Weiss fits on $M/H(T)$ data for filled skutterudite samples: external field [∞ =extrapolated by the Honda-Owen method (Ref. 47)], paramagnetic effective moment per Fe atom μ_{eff} (typical e.s.d. $0.05\mu_{\text{B}}$), and Weiss temperature Θ from the fit. The mass content of metallic iron impurity is derived from the difference of magnetization taken in fields of 35 kOe and 70 kOe.

Sample	H_{ext} [kOe]	$T_{\text{min/max}}$ [K]	μ_{eff} [μ_{B}]	Θ [K]	Fe content [$\mu\text{g/g}$]
NaFe ₄ Sb ₁₂ SPS bulk ^a	∞	150/400	1.76	+77.5(3)	≈ 600
NaFe ₄ Sb ₁₂ SPS bulk	∞	150/350	1.68	+76.4(4)	≈ 1000
NaFe ₄ Sb ₁₂ powder ^{b,c}	70	150/400	1.60	+87.9(1)	<5
KFe ₄ Sb ₁₂ SPS bulk	∞	150/400	1.66	+81.7(3)	≈ 500
KFe ₄ Sb ₁₂ powder ^c	70	150/400	1.67	+86.7(2)	<5
CaFe ₄ Sb ₁₂ SPS bulk ^b	∞	150/390	1.51	+45.7(5)	50
CaFe ₄ Sb ₁₂ powder ^c	70	150/400	1.51	+49.3(7)	10
BaFe ₄ Sb ₁₂ SPS bulk	∞	150/380	1.61	+9.9(4)	≈ 90
BaFe ₄ Sb ₁₂ powder ^c	∞	130/380	1.57	+15.0(9)	25–30

^aSample from Ref. 9 with lower density.

^bSample contained ca. 5 vol % Sb metal.

^cSample washed in HCl in order to remove the impurity of metallic Fe.

in 35 kOe and 70 kOe external fields (Honda-Owen method⁴⁷).

In order to remove the impurity, powder samples were washed in HCl. The field dependence of $\chi(T)$ of these purified materials is very small; thus, the ferromagnetic impurity was almost completely removed. Figure 9 demonstrates that the extrapolation method allows to extract the intrinsic susceptibility even for “impure” SPS material. Calculating the impurity content from the saturation magnetization of Fe (222 emu/g) a mass fraction of 5–30 $\mu\text{g/g}$ iron is found in the cleaned powders (see Table II). Unfortunately, by sintering, the impurity content increases again. The Fe metal content in SPS samples is estimated to be between 50 and ≈ 1000 $\mu\text{g/g}$.

Interestingly, for the purified KFe₄Sb₁₂ material, $\chi(T > 120$ K) is minimal for $H=20$ kOe and increases both for larger (35 kOe, 70 kOe; see Fig. 10, right panel) and smaller fields (10 kOe, influence of tiny residual iron impurities). This effect does not exist for the purified CaFe₄Sb₁₂ sample (Fig. 10, left panel), which displays only the influence of residual Fe metal impurities on $\chi(T)$. The increase of $\chi(T)$ above 20 kOe for KFe₄Sb₁₂ signals an increase of the para-

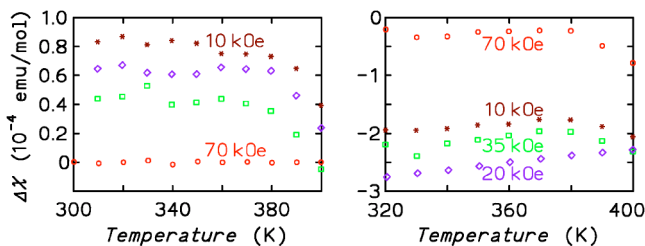


FIG. 10. (Color online) Field dependence of the susceptibility $\chi=M/H$ of purified powder samples of CaFe₄Sb₁₂ (left panel) and KFe₄Sb₁₂ (right panel). The differences $\Delta\chi$ to the respective Curie-Weiss fit of the susceptibility data taken in $H_{\text{ext}}=70$ kOe is shown (see text).

magnetic effective moment with field which may be due to a small dampening of spin fluctuations with increasing external field. These subtle effects, however, require further investigations.

From the magnetization data for Na and KFe₄Sb₁₂ the following picture evolves. Both alkali-metal skutterudites are weak itinerant electron ferromagnets with a small spontaneous magnetization which increases strongly with the applied field. Remarkably, the magnetic hysteresis behavior of Na/KFe₄Sb₁₂ is significantly harder than that of the half-metallic ferromagnets Co_{1-x}Fe_xS₂ with pyrite structure.⁴⁸

In the alkaline-earth-metal compounds CaFe₄Sb₁₂ and BaFe₄Sb₁₂ no magnetic phase transitions are observed down to 2 K (Figs. 11 and 12). SPS-treated material again shows the influence of ferromagnetic impurities in the paramagnetic susceptibility, but the iron contents are lower in the Ca and Ba compounds than in NaFe₄Sb₁₂ and KFe₄Sb₁₂ samples. However, even the purified powder sample of CaFe₄Sb₁₂ dis-

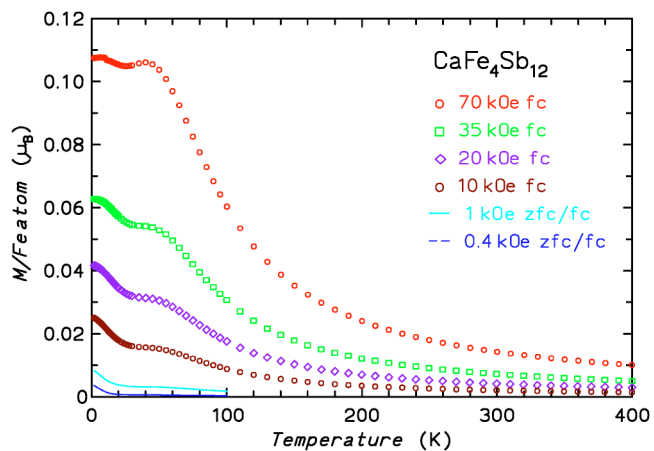


FIG. 11. (Color online) Magnetization per Fe atom versus temperature for different external magnetic fields for purified powder of CaFe₄Sb₁₂.

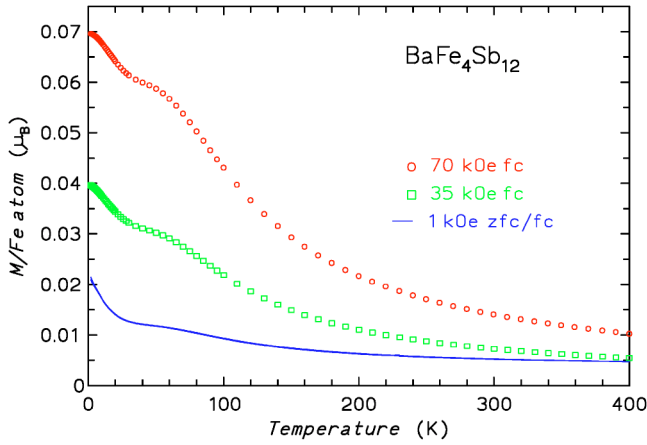


FIG. 12. (Color online) Magnetization per Fe atom versus temperature for different external magnetic fields for purified powder of $\text{BaFe}_4\text{Sb}_{12}$.

plays a change of slope at $T \approx 70$ K and a plateau in $\chi(T)$ around 40 K. In $\text{BaFe}_4\text{Sb}_{12}$ (Fig. 12) similar features also signal magnetic ordering phenomena. Upturns of the FC susceptibility for low external fields and much smaller ZFC signals may indicate precursor effects of ferromagnetic polarization below ca. 20 K in both compounds. The temperature of these features is approximately that of the Weiss temperatures Θ ; thus, the presence of a nearly ferromagnetic metallic state with strong spin fluctuations is indicated.

Summarizing, all our results indicate that a bulk ferromagnetic state exists only for the alkali-metal skutterudite compounds. Magnetization measurements in high magnetic fields up to 140 kOe on a $\text{CaFe}_4\text{Sb}_{12}$ powder sample (Fig. 7) show no sign of a possible itinerant electron-metamagnetic transition (see, e.g., Ref. 49) to a ferromagnetic state.

The high-field susceptibilities for purified samples are displayed in Fig. 13 in the H/M representation. The values resulting from fits of a Curie-Weiss law (least-squares fits to M/H) to these data in the paramagnetic range are given in Table II. The effective magnetic moments μ_{eff} per Fe atom are similar for alkali and alkaline-earth skutterudites, however, Ca and $\text{BaFe}_4\text{Sb}_{12}$ show slightly lower values than Na

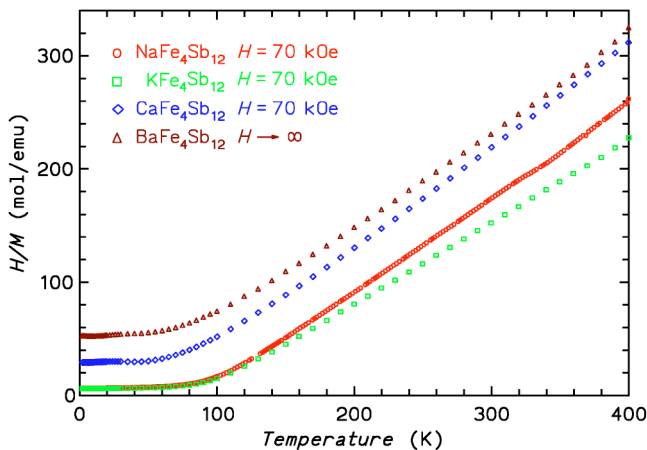


FIG. 13. (Color online) Inverse magnetic susceptibilities H/M of purified powder samples of filled skutterudites.

or $\text{KFe}_4\text{Sb}_{12}$. The apparent difference is the paramagnetic Weiss temperature: while all Θ are positive (ferromagnetic) and almost identical to the Curie temperature $T_C \approx 85$ K for the alkali-metal compounds, the Θ for the Ba compound is much smaller. For $\text{CaFe}_4\text{Sb}_{12}$ Θ is still remarkably large ($\Theta \approx 50$ K) whereas no sign of long-range order is detected.

The differences of our findings with the parameters μ_{eff} , Θ extracted in Ref. 11 for $\text{CaFe}_4\text{Sb}_{12}$ [$1.85(10)\mu_B$, $+3(1)$ K] and $\text{BaFe}_4\text{Sb}_{12}$ [$2.0(1)\mu_B$, $-36(1)$ K] from the susceptibility measurements in $H_{\text{ext}}=30$ kOe are probably due to the presence of ferromagnetic impurities in the samples which were not accounted for in the data evaluation. Due to the different preparation route, the amount of ferromagnetic iron impurities is often negligible in rare-earth-filled skutterudites.

In fact, $\text{LaFe}_4\text{Sb}_{12}$ has a significantly smaller $\mu_{\text{eff}}/\text{Fe atom}$ than the alkali- and alkaline-earth-filled skutterudites [$1.1\mu_B$ (Ref. 50), $1.12\mu_B$ (Ref. 46)], which fits in the observed trend of a smaller effective moment with increasing charge of the cation. As already pointed out,⁴⁶ a simple ionic model is inadequate since Fe-containing skutterudites are itinerant magnetic systems. Electrical resistivity measurements^{9,45} confirm that all four compounds are “bad metals” with room-temperature resistivities of 220–530 $\mu\Omega$ cm.⁵¹ As our calculations prove,^{9,44} naturally, the major part of the moment stems from the d -band polarization of the iron atoms and Sb atoms display a small counter-polarization.

Our observation of Curie-Weiss laws with similar values of μ_{eff} and different Θ is consistent with Moriya’s self-consistent renormalization (SCR) theory⁵² of weak itinerant ferromagnets. The behavior in the paramagnetic range is governed by spin fluctuations. The positive Θ values of both the alkali and alkaline-earth skutterudites are determined by the Stoner factor. As already discussed in our previous Letter, spin fluctuations play a crucial role in the formation of ferromagnetism in alkali and alkaline-earth metal iron antimony skutterudites.⁹ In the former compounds of Na and K the energy gain in the ferromagnetic state overcomes the impeding fluctuations while the smaller energy gain for alkaline-earth metal (Ca, Ba) skutterudites is insufficient for a static polarization of the d bands even at $T=2$ K. Presumably, the ferromagnetism depends on the subtle balance of dynamic and quantum-critical spin fluctuations,⁴⁴ as observed recently for other itinerant ferromagnets (see, e.g., Ref. 53). In fact, our recent investigations by nuclear magnetic resonance methods on ^{23}Na and ^{139}La nuclei suggest a changeover from weak itinerant ferromagnetism in $\text{NaFe}_4\text{Sb}_{12}$ to itinerant nearly antiferromagnetism in $\text{LaFe}_4\text{Sb}_{12}$,⁵⁰ according to the terminology of Moriya.⁵²

D. Mössbauer spectroscopy

The presence of the Mössbauer-active atoms ^{57}Fe and ^{121}Sb in the compounds under study enables us to explore their local surrounding and nuclear hyperfine parameters.

The room-temperature ^{57}Fe Mössbauer spectrum of $\text{NaFe}_4\text{Sb}_{12}$ (Fig. 14) is a paramagnetic doublet with isomer shift $\delta(\text{Fe})=0.258(4)$ mm s^{-1} , quadrupole splitting $\Delta E_Q(\text{Fe})=0.21(1)$ mm s^{-1} , and linewidth 0.256(7) mm s^{-1} . These val-

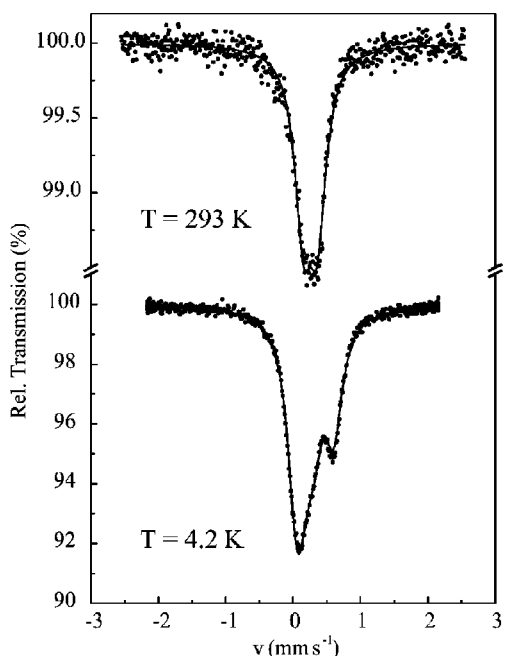


FIG. 14. ^{57}Fe Mössbauer spectra of $\text{NaFe}_4\text{Sb}_{12}$ recorded at 293 K and at 4.2 K K.

ues correspond formally to a ferriclike oxidation state of iron, which is surrounded by six antimony atoms forming a distorted octahedron. A comparison with literature data,⁵⁴ where a correlation of $\Delta E_Q(\text{Fe})$ with the distortion of almost square Sb_4 units (Fig. 3) was sought for, shows a similar ^{57}Fe quadrupole splitting for $\text{Tl}_{0.8}\text{Co}_3\text{FeSb}_{12}$. No lines of elemental iron were visible in the spectrum. At $T=4.2$ K a weak hyperfine magnetic field $H_{\text{hf}}(\text{Fe})=16.4(1)$ kOe is detected on the iron nuclei (Fig. 14) in agreement with the bulk ferromagnetism⁵⁵ from magnetization data. The isomer shift and quadrupole splitting extracted from the magnetically split spectrum are $\delta(\text{Fe})=0.379(2)$ mm s^{-1} and $\epsilon(\text{Fe})=0.09(1)$ mm s^{-1} , respectively.

The antimony Mössbauer spectra recorded at 150 K and 4.2 K are shown in Fig. 15. The positions of Mössbauer lines of Sb_2O_3 , Sb_2O_5 and metallic Sb measured at 4.2 K are indicated by arrows. These lines provide the isomer shift reference scale. Corresponding values of isomer shifts relative to the source ^{121m}Sn (CaSnO_3) are $\delta(\text{Sb}_2\text{O}_3)=-11.65(2)$ mm s^{-1} , $\delta(\text{Sb})=-10.84(2)$ mm s^{-1} , and $\delta(\text{Sb}_2\text{O}_5)=0.57(2)$ mm s^{-1} .

At 150 K a paramagnetic antimony spectrum with $\delta(\text{Sb})=-10.03(2)$ mm s^{-1} and $\Delta E_Q(\text{Sb})=6.0(6)$ mm s^{-1} (Fig. 15) is observed. The spectrum confirms the existence of only one crystallographic site of antimony. $\Delta E_Q(\text{Sb})$ is in the range of shifts of the oxide Sb_2O_3 and of metallic antimony. This large value of $\Delta E_Q(\text{Sb})$ indicates a local surrounding of low symmetry where Sb is coordinated by two Sb and two Fe atoms which form a distorted tetrahedron. A similar pronounced magnitude of the quadrupole interaction was observed in the binary skutterudite CoSb_3 .⁵⁶ The presence of this distortion agrees well with results of ^{121}Sb nuclear quadrupole resonance (NQR) measurements.⁵⁷ The weak broadened line with relative intensity about 5% seen at $T=4.2$ K at

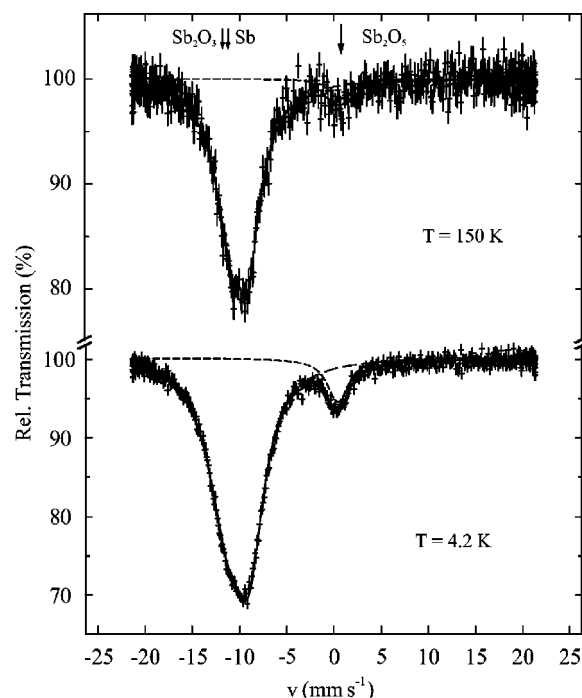


FIG. 15. ^{121}Sb Mössbauer spectra of $\text{NaFe}_4\text{Sb}_{12}$ measured at 150 K and 4.2 K. Line positions of reference antimony compounds are shown by arrows.

$0.41(11)$ mm s^{-1} can be attributed to an Sb_2O_5 impurity. Since the sample for the Mössbauer measurement was not washed in HCl, Sb_2O_5 is most likely a product of hydrolysis of intermediate sodium-antimonides in the material.

Upon cooling, the fit for the ^{121}Sb Mössbauer spectrum of $\text{NaFe}_4\text{Sb}_{12}$ reveals a small magnetic hyperfine splitting $H_{\text{hf}}(\text{Sb})=10.4(16)$ kOe, reflecting the ferromagnetic state. This polarization of nonmagnetic antimony atoms is also a characteristic of the itinerant magnetism in the skutterudites.

Applying an external field of 16 kOe the value of the effective field H_{hf} on the iron nuclei increased to ca. 32 kOe. This result is surprising, insofar as in the ferromagnetic state a decrease of the effective field could be expected. Normally, the Fermi contact term H_F dominates in the expression describing the hyperfine field on the Mössbauer nucleus in a metallic ferromagnet:

$$H_{\text{hf}} = H_{\text{ext}} + H_F + H_B + H_D + H_{\text{DM}} + H_L + H_{\text{cond}},$$

where H_{ext} is the external magnetic field. The Fermi contact term H_F (negative) originates from the imbalance of spin density of core s electron polarized by unpaired d electrons. However, the LDA calculation (see above and Ref. 44) shows that, in $\text{NaFe}_4\text{Sb}_{12}$, the polarization of the Fe $4s$ electrons is positive ($+0.00668\mu_B$; $3s$ polarization is negligible)—i.e., has the same sign as the $3d$ electron polarization. In order to understand this the remaining terms have to be analyzed. Both the orbital term H_B and the dipole term H_D , arising from the dipolar interaction of the nucleus with the spin moment of the atom, are positive. The demagnetizing field H_{DM} and the Lorentz field H_L are both small. The polarized conduction electron contribution through the Fermi

contact interaction H_{cond} is positive. There are no general theoretical estimates for the magnitude of this contribution, but it might be relatively large [≈ 100 kOe (Ref. 58)]. However, in the case of half-metallic magnets, direct conduction electron polarization may be important. One cannot exclude that the sum of the dominant positive terms $H_{\text{B}} + H_{\text{cond}}$ will prevail in this crude estimation of H_{hf} in half-metallic ferromagnets. As a result, in an external magnetic field the observed hyperfine field could increase. Another reason leading to the increase of the hyperfine field might be the damping of spin fluctuations in external magnetic field (see above).

IV. CONCLUSIONS

Detailed chemical analysis and XRD crystal structure investigation show full occupancy of the sodium position in the $\text{NaFe}_4\text{Sb}_{12}$ structure. No indication for off-center displacement for Na atoms is found. Only a dynamical thermal motion is present for Na. The chemical bonding is analyzed within the concept of the electron localization function. This analysis reveals a strong covalent character of the Fe-Sb and Sb-Sb interactions in the polyanion $[\text{Fe}_4\text{Sb}_{12}]^{0.98-}$ and an almost complete transfer of charge from sodium to the polyanion. The value of the bulk modulus [$B_0 = 85(1)$ GPa] of $\text{NaFe}_4\text{Sb}_{12}$ is lower than that of IrSb_3 , consistent with even stronger covalent bonding in the latter skutterudite. The electronic structure is characterized by a ferromagnetic ground state with a large spin polarization of 99% and, therefore, almost perfect half-metallic behavior. Indeed, from electrical

resistivity data the filled skutterudites of Na, K, Ca, and Ba are bad metals.

The weak itinerant ferromagnetism of $\text{NaFe}_4\text{Sb}_{12}$ and $\text{KFe}_4\text{Sb}_{12}$ is characterized by a rather high Curie temperature and by small ordered magnetic moments which increase strongly with the external field. The paramagnetic susceptibilities of the alkaline-earth skutterudites as well as of the alkali skutterudites both follow Curie-Weiss laws with almost identical effective magnetic moment. These observations demonstrate the presence of strong spin fluctuations in the sense of the SCR theory of Moriya. From an experimental point of view, $\text{NaFe}_4\text{Sb}_{12}$ and $\text{KFe}_4\text{Sb}_{12}$ behave almost identical. $\text{CaFe}_4\text{Sb}_{12}$ and $\text{BaFe}_4\text{Sb}_{12}$ are paramagnetic (nearly ferromagnetic⁵²) down to 2 K, in spite of sizable Weiss temperatures from Curie-Weiss fits to the high-temperature susceptibility. In $\text{CaFe}_4\text{Sb}_{12}$ and $\text{BaFe}_4\text{Sb}_{12}$ the energy gain in the ferromagnetic state is insufficient to overcome the spin fluctuations. They can be addressed as nearly ferromagnetic metals. By Mössbauer spectroscopy small hyperfine fields at the iron and antimony sites were detected which are in agreement with the weak d -band polarization. The hyperfine field of iron is found to be parallel to the Fe d -shell polarization.

ACKNOWLEDGMENTS

We are indebted to G. Auffermann (powder neutron diffraction), R. Cardoso-Gil (x-ray diffraction), N. Reinfried (SPS treatments), and M. Hanfland (ESRF Grenoble, high-pressure XRD). A.R. acknowledges the Zeit-Stiftung and H.R. the Deutsche Forschungsgemeinschaft (Emmy-Noether-Programm) for financial support.

*Electronic address: jasper@cpfs.mpg.de

[†]Permanent address: Moscow State University, Faculty of Physics, Moscow, Russia.

[‡]Permanent address: Kamerlingh Onnes Laboratory, Leiden University, Leiden, The Netherlands.

¹A. Breithaupt, *Ann. Phys. (Leipzig)* **9**, 115 (1827).

²W. Jeitschko and D. Braun, *Acta Crystallogr., Sect. B: Struct. Crystallogr. Cryst. Chem.* **33**, 3401 (1977).

³C. Uher, *Semicond. Semimetals* **68**, 139 (2001).

⁴I. Shirovani, Y. Shimaya, K. Kihou, C. Sekine, N. Takeda, M. Ishikawa, and T. Yagi, *J. Phys.: Condens. Matter* **15**, S2201 (2003).

⁵E. D. Bauer, N. A. Frederick, P.-C. Ho, V. S. Zapf, and M. B. Maple, *Phys. Rev. B* **65**, 100506(R) (2002).

⁶N. A. Frederick, T. D. Do, P.-C. Ho, N. P. Butch, V. S. Zapf, and M. B. Maple, *Phys. Rev. B* **69**, 024523 (2004).

⁷G. A. Slack and V. G. Tsoukala, *J. Appl. Phys.* **76**, 1665 (1994).

⁸B. C. Sales, in *Handbook on the Physics and Chemistry of Rare Earths*, edited by K. A. Gschneidner, Jr., J.-C. G. Bünzli, and V. K. Pecharsky (Elsevier, Amsterdam, 2003), Vol. 33, Chap. 211, pp. 1–34.

⁹A. Leithe-Jasper, W. Schnelle, H. Rosner, N. Senthilkumaran, A. Rabis, M. Baenitz, A. Gippius, E. Morozova, J. A. Mydosh, and Y. Grin, *Phys. Rev. Lett.* **91**, 037208 (2003).

¹⁰J. M. D. Coey and S. Sanvito, *J. Phys. D* **37**, 988 (2004).

¹¹M. E. Danebrock, C. B. Evers, and W. Jeitschko, *J. Phys. Chem. Solids* **57**, 381 (1996).

¹²M. Tokita, *J. Soc. Powder Technol. Jpn.* **30**, 790 (1993).

¹³G. K. White and M. L. Minges, *Int. J. Thermophys.* **18**, 1269 (1997).

¹⁴L. G. Akselrud, P. Y. Zavalii, Y. Grin, V. K. Pecharsky, B. Baumgartner, and E. Wölfel, *Mater. Sci. Forum* **133-136**, 335 (1993).

¹⁵G. M. Sheldrick, computer code SHELXL-97, University of Göttingen, Göttingen, 1997.

¹⁶K. Lagarec and D. G. Rancourt, *Nucl. Instrum. Methods Phys. Res. B* **129**, 266 (1997).

¹⁷H. Spiering, L. Deák, and L. Böttlyán, *Hyperfine Interact.* **125**, 197 (2000); <ftp://iacgu7.chemie.uni-mainz.de/pub/effi>

¹⁸O. Jepsen, A. Burkhardt, and O. Andersen, computer code TB-LMTO-ASA version 4.7, Max-Planck-Institut für Festkörperforschung, Stuttgart, 1999.

¹⁹U. Barth and L. Hedin, *J. Phys. C* **5**, 1629 (1972).

²⁰O. K. Andersen, *Phys. Rev. B* **12**, 3060 (1975).

²¹A. Savin, A. D. Becke, J. Flad, R. Nesper, H. Preuss, and H. G. von Schnering, *Angew. Chem., Int. Ed. Engl.* **30**, 409 (1991).

²²A. Savin, O. Jepsen, J. Flad, O. K. Andersen, H. Preuss, and H. G. von Schnering, *Angew. Chem., Int. Ed. Engl.* **31**, 187 (1992).

²³M. Kohout, computer code BASIN, version 2.3, Max-Planck-Institut für Chemische Physik fester Stoffe, Dresden, 2001.

²⁴R. F. W. Bader, *Atoms in Molecules: A Quantum Theory* (Oxford

- University Press, Oxford, 1999).
- ²⁵K. Koepf and H. Eschrig, Phys. Rev. B **59**, 1743 (1999).
- ²⁶J. P. Perdew and Y. Wang, Phys. Rev. B **45**, 13 244 (1992).
- ²⁷H. Eschrig, *Optimized LCAO Method and the Electronic Structure of Extended Systems* (Springer, Berlin, 1989).
- ²⁸C. B. H. Evers, L. Boonk, and W. Jeitschko, Z. Anorg. Allg. Chem. **620**, 1028 (1994).
- ²⁹N. T. Stetson, S. M. Kauzlarich, and H. Hope, J. Solid State Chem. **91**, 140 (1991).
- ³⁰C. B. H. Evers, W. Jeitschko, L. Boonk, D. J. Braun, T. Ebel, and U. Scholz, J. Alloys Compd. **224**, 184 (1995).
- ³¹B. C. Chakoumakos, B. C. Sales, D. Mandrus, and V. Keppens, Acta Crystallogr., Sect. B: Struct. Sci. **55**, 341 (1999).
- ³²M. D. Hornbostel, E. J. Hyer, J. H. Edvalson, and D. C. Johnson, Inorg. Chem. **36**, 4270 (1997).
- ³³D. Cao, F. Bridges, S. Bushart, E. D. Bauer, and M. B. Maple, Phys. Rev. B **67**, 180511(R) (2003).
- ³⁴The difference electron density was studied based on single-crystal XRD data ($T=295$ K). For that purpose a difference Fourier synthesis based on $|F_o| - |F_c|$ was calculated with the Na atom removed from the refined model.
- ³⁵J. L. Feldman, D. J. Singh, I. I. Mazin, D. Mandrus, and B. C. Sales, Phys. Rev. B **61**, R9209 (2000).
- ³⁶J. L. Feldman, D. J. Singh, C. Kendziora, D. Mandrus, and B. C. Sales, Phys. Rev. B **68**, 094301 (2003).
- ³⁷T. Caillat, A. Borshchevsky, and J. Fleurial, J. Appl. Phys. **80**, 4442 (1996).
- ³⁸F. D. Murnaghan, Proc. Natl. Acad. Sci. U.S.A. **30**, 244 (1944).
- ³⁹U. Schwarz, M. Schmidt, R. Gumenuik, W. Schnelle, M. Hanfland, K. Klementiev, and Y. Grin, Z. Anorg. Allg. Chem. **630**, 122 (2004).
- ⁴⁰T. S. Snider, J. V. Badding, S. B. Schujman, and G. A. Slack, Chem. Mater. **12**, 697 (2000).
- ⁴¹M. Kohout, F. R. Wagner, and Y. Grin, Theor. Chem. Acc. **108**, 150 (2002).
- ⁴²ELF-hompage <http://www.cfps.mpg.de/ELF/index.html>
- ⁴³M. Kohout and A. Savin, Int. J. Quantum Chem. **60**, 875 (1996).
- ⁴⁴H. Rosner *et al.* (unpublished).
- ⁴⁵W. Schnelle *et al.* (unpublished).
- ⁴⁶D. Ravot, U. Lafont, L. Chapon, J. Tedenac, and A. Mauger, J. Alloys Compd. **323-324**, 389 (2001).
- ⁴⁷K. Honda, Ann. Phys. (Leipzig) **32**, 1027 (1910).
- ⁴⁸K. Ramesha, R. Seshadri, C. Ederer, T. He, and M. A. Subramanian, Phys. Rev. B **70**, 214409 (2004).
- ⁴⁹N. V. Mushnikov and T. Goto, J. Phys.: Condens. Matter **11**, 8095 (1999).
- ⁵⁰A. A. Gippius *et al.* (unpublished).
- ⁵¹The electrical resistivity of polycrystalline samples strongly depends on their porosity which can be effectively reduced by SPS treatment (see, e.g., Ref. 59). Previous samples had resistivities of order $1500 \mu\Omega \text{ cm}$ at 300 K.
- ⁵²T. Moriya, *Spin Fluctuations in Itinerant Electron Magnetism* (Springer-Verlag, Berlin, 1985).
- ⁵³A. Aguayo, I. I. Mazin, and D. J. Singh, Phys. Rev. Lett. **92**, 147201 (2004).
- ⁵⁴G. J. Long, B. Mathieu, B. C. Sales, R. P. Hermann, and F. Grandjean, J. Appl. Phys. **92**, 7236 (2002).
- ⁵⁵Mössbauer spectroscopy is insensitive to spin fluctuations on a time scale of 10^{-8} s or faster.
- ⁵⁶I. Lefebvre-Devos, M. Lassalle, X. Wallart, J. Olivier-Fourcade, L. Monconduit, and J. C. Jumas, Phys. Rev. B **63**, 125110 (2001).
- ⁵⁷A. Rabis, A. Leithe-Jasper, A. A. Gippius, E. Morozova, M. Baenitz, W. Schnelle, N. Senthilkumaran, J. A. Mydosh, F. Steglich, and Y. Grin, J. Magn. Magn. Mater. **272-276**, 830 (2004). The hyperfine field values for the Na site have to be multiplied by 0.1 (in print); Phys. Rev. Lett. **93**, 089904(E) (2004).
- ⁵⁸*Chemical Applications of Mössbauer Spectroscopy*, edited by V. I. Goldanskii (Academic Press, New York, 1968).
- ⁵⁹L. Yang, J. S. Wu, and L. T. Zhang, J. Alloys Compd. **364**, 83 (2003).